U₈Al₁₉Si₆, A Uranium Aluminide Silicide with a Stuffed Supercell Grown from Aluminum Flux

Wesley M. Potter,[§] You Lai,[†,⊥] Huibo Cao,[‡] Ryan E. Baumbach,[†,⊥] and Susan E. Latturner[*,§]

[§]Department of Chemistry and Biochemistry, Florida State University, Tallahassee, Florida 32306, United States
[†]Department of Physics, Florida State University, Tallahassee, Florida 32306, United States
[‡]Neutron Scattering Division, Oak Ridge National Laboratory, Oak Ridge, Tennessee 37831, United States
[⊥]National High Magnetic Field Lab, Florida State University, Tallahassee, Florida 32310, United States

Ⓢ *Supporting Information*

ABSTRACT: $U_8Al_{19}Si_6$ is formed from the reaction of uranium oxide and silicon in aluminum flux. Growth of this material is dependent on the presence of surface hydroxyl groups on alumina in the crucible. The compound forms as large cuboid crystals with a complex new structure that is a cubic stuffed supercell of UAl_3 ($AuCu_3$ parent structure type). It features a 4-fold expansion of the unit cell axis and the addition of atoms on two extra positions resulting in $Pm\bar{3}n$ symmetry. The ordered distribution of aluminum and silicon was determined using single crystal neutron diffraction. The magnetic susceptibility shows temperature independent paramagnetic behavior, while heat capacity measurements are consistent with Fermi liquid characteristics at low temperatures where the Sommerfeld constant is enhanced in comparison to that of a conventional metal. These bulk thermodynamic properties indicate that $U_8Al_{19}Si_6$ is an itinerant electron Pauli paramagnet with moderately enhanced mass charge carrier quasiparticles.

INTRODUCTION

The U−Al−Si system is of great interest due to its technological importance. For example, the uranium fuel rods in the BR1 nuclear reactor in Belgium (active since 1956) contain natural uranium slugs clad in aluminum. In the cladding process, silicon is added as an impurity to create a $U(Al,Si)_3$ layer that prevents the interdiffusion of uranium and aluminum.[1] Uranium oxide is also used as a fuel in cermet (ceramic/metal) reactors, dispersed into a metal matrix such as aluminum or molybdenum.[2,3] To understand the behavior of these nuclear fuels (and facilitate their treatment as waste, once spent), it is important to know what potential binary and ternary phases might form at the interface of the uranium or uranium oxide and the surrounding metal cladding or matrix.

Reactions of uranium or uranium oxide in aluminum flux will shed light on possible phases occurring at U/Al interfaces and offer insight into the quasi-binary UAl_3−USi_3 system. Metal flux reactions use a low melting metal or metal mixture in which reactants dissolve and react with one another. Metal fluxes have proven to be highly effective media for crystal growth of a wide variety of complex intermetallics.[4−7] Aluminum is quite often a reactive solvent when used as a flux—it is commonly incorporated into products. This, and the high solubility and reactivity of most elements in molten aluminum, leads to the formation of multinary intermetallics such as $Ca_3Au_{6+x}Al_{26}Ti$,

$Yb_{2.77}FeAl_{3.72}Mg_{0.28}Si_2$, $YbAu_4Al_8Si$, and $Gd_5Mg_5Fe_4Al_{12}Si_8$ from aluminum flux reactions.[8−11] Another very useful aspect of molten aluminum is its strong reducing power; this allows oxides to be used as reactants. For instance, reactions of ThO_2 with Au and Si in aluminum flux led to three structurally related products—$Th_2AuAl_2Si_3$, $Th_2Au_3Al_4Si_2$, and $Th_2Au_5Al_8Si_2$.[12]

UAl_3 and USi_3 both have the cubic $AuCu_3$ structure type ($Pm\bar{3}m$).[13] The uranium site is 12 coordinate, with all surrounding U−X bond lengths identical (3.017 Å for UAl_3; 2.853 Å for USi_3). Since UAl_3 is isostructural with USi_3 (unit cell parameters a = 4.2651 Å and a = 4.0348 Å, respectively), one might expect the $UAl_{3−x}Si_x$ system to be isomorphous and to follow Vegard's law. However, several studies indicate a nonlinear relationship between substitution and unit cell parameters and a potential miscibility gap and supercell formation.[14−16] In addition to interesting crystal chemistry, the $UAl_{3−x}Si_x$ system is also of interest for its magnetic properties, which result from variations in the uranium f-electron bandwidth and hybridization. USi_3 displays temperature independent paramagnetism, UAl_3 exhibits spin fluctua-

Figure 1. Microscope images of $U_8Al_{19}Si_6$ crystals grown from aluminum flux. (a) The single crystal used for neutron diffraction experiment under Parabar oil on 1 mm grid paper. (b) A cuboid crystal showing aluminum oxide residue after NaOH etching. (c) Crystals growing off of a piece of alumina cement.

tions, and certain compositions of $UAl_{3-x}Si_x$ are reported to become superconducting at low temperatures.[17−19]

In this work, we have discovered a new stuffed supercell variant of $UAl_{3-x}Si_x$ that forms when uranium oxide reacts with silicon in aluminum flux in the presence of high surface area alumina. This new stuffed superstructure ($U_8Al_{19}Si_6$ [Z = 8], $Pm\bar{3}n$) has a 4-fold expansion of the unit cell edge and two extra occupied sites that produce a U:(Al/Si) ratio of 1:3.125 instead of the expected 1:3. The ordered aluminum and silicon siting were determined by single crystal neutron diffraction. Magnetic susceptibility measurements reveal nearly temperature independent behavior across the entire measured range. Heat capacity measurements at low temperatures are consistent with Fermi liquid behavior, where the Sommerfeld constant is enhanced by comparison to that of a conventional metal. These properties are similar to what is seen for the parent compound UAl_3.[19]

■ EXPERIMENTAL PROCEDURE

Caution: All the uranium compounds used in these studies contained depleted uranium; nonetheless, standard precautions were performed for handling radioactive materials.

Synthesis. Silicon powder (Strem Chemicals, 99+%), uranium dioxide powder (Gallard-Schlesinger Chemical Mfg. Corp., 99.95%), and aluminum slugs (3.125 mm diameter × 6.35 mm length, Alfa-Aesar, 99.99%) were combined in alumina crucibles in 1−5:0.5:30 mole ratios. The alumina crucibles were made from alumina tubing (Coorstek, 0.7 cm ID, 5 cm length) open-ended on the top and closed with cement on the bottom (Applied Test Systems, Inc. EA139 alumina embedding cement was baked onto the bottom of the crucibles overnight at 1000 °C). The loaded crucibles were placed in fused silica tubes and sealed under vacuum (~90 mTorr). The ampules were heated in a box furnace to 1000 °C in 12 h, held at 1000 °C for 24 h, cooled to 660 °C in 48 h, and then cooled to room temperature by turning the furnace off. The crucibles were then removed from the silica tubes and put into a 5 M NaOH solution overnight to etch the Al flux from the products. The NaOH solution was removed via three washes with DI water followed by one wash with acetone. The crystals removed from the alumina crucibles were cuboids coated with a white oxide powder (see Figure 1).

In addition to etching with NaOH, separation of crystals from flux via centrifugation was explored. In this method the same reaction ratios and vacuum sealing were employed; however, a wad of quartz wool was placed in the silica tube approximately 2−3 cm above the alumina crucible (before vacuum sealing) to act as a filter during the subsequent centrifugation process. These reactions were heated to 1000 °C in 12 h, held at 1000 °C for 24 h, then cooled to 800 °C in 48 h, and then centrifuged at that temperature. During the centrifugation process, the reactions are quickly taken out of the furnace (while the flux is still molten), inverted, and centrifuged for 1 min. In this process, the liquid flux runs through the quartz wool while the crystals adhere

to the inside of the alumina crucible. Reactions centrifuged at 750 °C yielded no solid product, indicating that $U_8Al_{19}Si_6$ crystallizes below this temperature.

Elemental Analysis: SEM-EDS. Elemental analysis was performed on samples using a FEI NOVA 400 scanning electron microscope coupled with energy-dispersive X-ray spectroscopy (SEM-EDS). Flux-grown crystals were affixed to an aluminum SEM-EDS puck using double-sided carbon tape, cleaved with a razor blade to expose inside surfaces, and positioned so that the cleaved surfaces were perpendicular to the electron beam. Analysis of all samples used 30 kV accelerating voltage and an accumulation time of 60s. The majority of samples analyzed showed atomic percentages in the following ranges: U = 25−29%, Al = 51−54%, and Si = 17−24%.

Structural Characterization: X-ray Diffraction. A large crystal that had been previously analyzed by SEM-EDS was placed in Parabar oil (Hampton Research) and broken into smaller pieces with a razor blade under a light microscope. A roughly spheroidal fragment was selected and affixed to a MiTeGen tip (using the Parabar oil as adhesive). Single crystal X-ray diffraction (SC-XRD) data were collected at 158 K using a Bruker APEX 2 CCD diffractometer with a Mo Kα radiation source. The data were processed using the SHELXTL software package.[20] The structure was refined in cubic space group $Pm\bar{3}n$; data collection and refinement parameters are found in Table 1. All light atom sites were initially refined as aluminum; since aluminum and silicon cannot be distinguished by XRD, selected sites were assigned as silicon based on the presence of shorter distances to nearby uranium sites. Because of the larger difference in neutron scattering factors for aluminum and silicon, neutron diffraction was carried out to determine Al and Si siting (see below). Powder X-ray diffraction data were also collected at room

Table 1. Crystallographic Information and Data Collection Parameters for $U_8Al_{19}Si_6$ Crystals

	$U_8Al_{19}Si_6$, X-ray data (crystal 1)	$U_8Al_{19}Si_6$, X-ray and neutron data (crystal 2)
space group		$Pm\bar{3}n$
cell edge (Å)	16.805(1)	16.835(2)
V (Å^3)	4746.0(7)	4771.2(8)
Z		8
density, theor. (g/cm^3)	7.237	7.198
radiation, wavelength (Å)	0.71073	0.71073
temperature (K)	158	150
reflections	83885	78924
unique reflections	1338	1339
data/parameters	1338/66	1339/66
μ (mm^{-1})	55.40	55.10
R_1/wR_2 ($I > 2\sigma(I)$)	0.0154/0.0331	0.0282/0.0692
R_1/wR_2 (all data)	0.0398/0.0405	0.0400/0.0756
largest residual peak/hole (e·Å^{-3})	1.34/−1.09	2.36/−1.88

Table 2. Atom Positions, Thermal Parameters (from SCXRD data collected at 150 K), and Site Occupancies (from neutron diffraction at 150 K) for $U_8Al_{19}Si_6$ [a]

atom	Wyckoff site	x	y	z	occupancy	U_{eq}
U1	48l	0.38161(2)	0.36641(2)	0.11825(2)	1	0.0013(1)
U2	16i	0.38234(2)	0.38234(2)	0.38234(2)	1	0.0013(1)
Si1	12f	1/2	0.3449(2)	1/2	1	0.0015(6)
Si2	24k	0.3436(2)	0.2512(2)	0	1	0.0024(5)
Si3	12g	1/2	0.4062(2)	0	1	0.0021(7)
Al1	24k	0.2445(2)	0.3776(2)	0	1	0.0026(6)
Al2	12f	1/2	1/2	0.1318(2)	1	0.0017(7)
Al3	24k	0.2487(2)	0.1267(2)	0	0.86(8) Al/0.14(8) Si	0.0021(5)
Al4	24k	0.1266(2)	0.2565(2)	0	1	0.0020(6)
Al5	48l	0.2431(1)	0.2506(1)	0.1265(1)	1	0.0028(4)
Al6	12h	0.1298(3)	1/2	0	1	0.0024(8)
Al7	6c	1/2	1/4	0	1	0.004(1)
Al8	2a	1/2	1/2	1/2	0.91(5) Al	0.005(2)

[a] U_{eq} is defined as one third of the trace of the orthogonalized U_{ij} tensor.

temperature on ground up reaction products using a PANalytical X'Pert PRO powder diffractometer with a Cu Kα radiation source. The resulting powder patterns were compared to the pattern calculated based on the structure derived from the single crystal diffraction study (see Figure S1 in Supporting Information).

Neutron Diffraction. Neutron diffraction data were collected on a single crystal (spheroidal, 2 mm in diameter; see Figure 1) at the four-circle diffractometer HB-3A at the High Flux Isotope Reactor at Oak Ridge National Laboratory. Data were collected at 150 K with the neutron wavelength of 1.546 Å from a bent perfect Si-220 monochromator.[21] A pyrolytic graphite filter was used to remove the λ/2 neutrons. The structure refinement was carried out using FullProf and was based on 150 merged reflections.[22] To facilitate accurate refinement of site occupancies, single crystal X-ray diffraction data were collected at 150 K (method as described above) for a fragment of the same crystal. The positions and thermal parameters from the SCXRD structure refinement were used in the refinement of the neutron diffraction data. The occupancies were the only parameters to be refined with the neutron data. With the exception of the Al3 and Al8 sites, all light element sites were 100% occupied by one element within standard deviation; their occupancies were therefore fixed to 100%. Details of these data collections are listed in Table 1. Resulting atom positions and occupancy parameters are shown in Table 2.

Magnetization and Heat Capacity Measurements. Temperature- and field-dependent magnetization measurements were carried out on several individual single crystals at temperatures from 1.8−300 K under an applied magnetic field of 1 kOe using a Quantum Design VSM Magnetic Property Measurement System (see Figure S2, Supporting Information). Heat capacity data were collected from 1.8−120 K using a Quantum Design Physical Property Measurement System. These measurements were performed at the National High Magnetic Field Laboratory DC field user facility using standard cryostats.

RESULTS AND DISCUSSION

Synthesis. The flux reaction that produces $U_8Al_{19}Si_6$ is dependent on two unusual parameters. Uranium oxide (UO_2) is required as a reactant; the aluminum flux acts as both a solvent and a reducing agent. If uranium metal is used instead, a $U(Al_{3−x}Si_x)$ product with a previously reported tetragonal supercell is formed ($I4/mmm$, a = 8.3471 Å, c = 16.8089 Å).[14,15] Another crucial synthesis parameter is the presence of high surface area alumina. The alumina crucibles used in this work are formed from 5 cm lengths of alumina tubing that are closed on the bottom with a plug of alumina cement; this cement is applied and then fired at 1000 °C. The product

appears to grow from the surface of this cement. If it is not present (if cast alumina crucibles are used), only solids with the UAl_3 structure ($Pm\overline{3}m$, a = 4.2 Å) are formed. If cast alumina crucibles are used but pieces of fired cement are added, $U_8Al_{19}Si_6$ is formed; the crystals grow off the piece of added cement (see Figure 1c). Representative pieces of this fired cement were analyzed by elemental analysis and powder XRD. These data indicate it is comprised of Al_2O_3 in the rhombohedral α-phase ($R3c$). This is identical to the composition of the crucible body.

Many examples of reaction of a metal flux with a crucible material have been reported. This can either be detrimental, leading to contamination of desired products, or adventitious, leading to unexpected new materials.[23] Some recent examples of the latter are the leaching of iron out of steel crucibles, which produced an unusual nitridoferrate(I) $Ca_6(Li_xFe_{1−x})Te_2N_3$, and the partial reduction of alumina crucibles by a strongly reducing rare-earth based flux, which produced $Nd_8Co_{4−x}Al_xGe_2C_3$.[24,25] However, this synthesis of $U_8Al_{19}Si_6$ is notable in that it appears that it is the surface composition of the alumina that is critical. This may be due to the higher surface area and concentration of hydroxyl groups on the surface of the alumina cement, compared to the denser walls of the crucible. To further test this, reactions were carried out in cast crucibles with no cement, but with alumina powder added: either 0.5 or 3 mmol of Al_2O_3 (Alfa-Aesar, 99.99%, 40 μm) added to a 0.5:3:30 mmol UO_2/ Si/Al flux ratio. Reactions with 0.5 mmol of Al_2O_3 powder produced the tetragonal $U(Al_{3−x}Si_x)$ compound; when 3 mmol of powdered Al_2O_3 was present, large crystals of $U_8Al_{19}Si_6$ were produced. There is a strong likelihood that the higher content of surface hydroxyl groups on the powder or cement versus the cast alumina body plays a role in promoting the formation of the title phase. The effects of hydroxylation of alumina surfaces have been widely studied in the deposition of metal films and growth of metal nanoclusters for preparation of heterogeneous catalysts, with the consistent observation that metals wet and adhere to hydroxylated surfaces much more strongly than to dehydroxylated surfaces.[26−28] While the mechanism for $U_8Al_{19}Si_6$ growth from flux is not known, it appears that interaction with surface hydroxyl groups on alumina plays a role. This introduces the possibility that this compound contains interstitial oxide or hydride anions that stabilize it. However, neutron diffraction data showed no evidence of extensive incorporation of these species (vide infra).
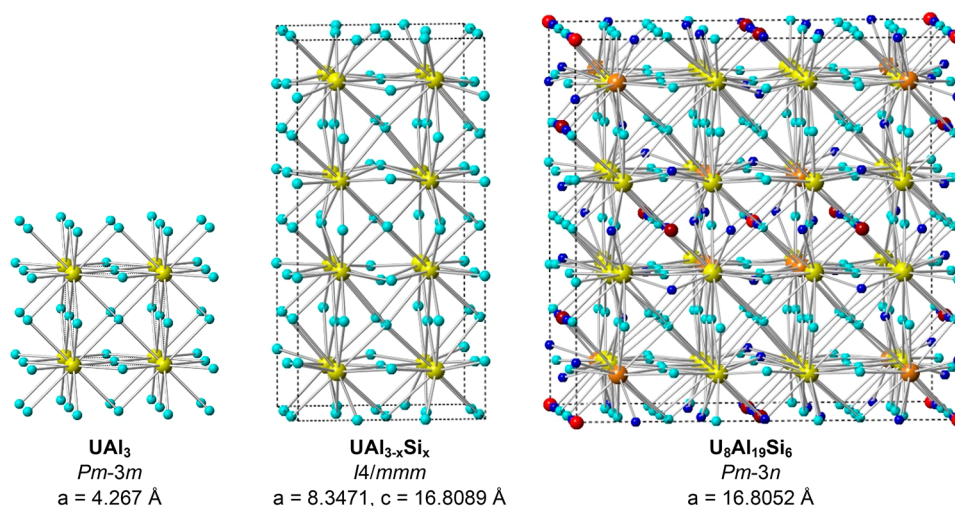
Figure 2. Comparison of the crystal structures of UAl_3, tetragonal $U(Al_{3-x}Si_x)$ supercell, and the $U_8Al_{19}Si_6$ stuffed superstructure. Uranium atoms are large yellow spheres, and aluminum and silicon are smaller light and dark blue spheres, respectively. Stuffed sites in $U_8Al_{19}Si_6$ are red spheres.
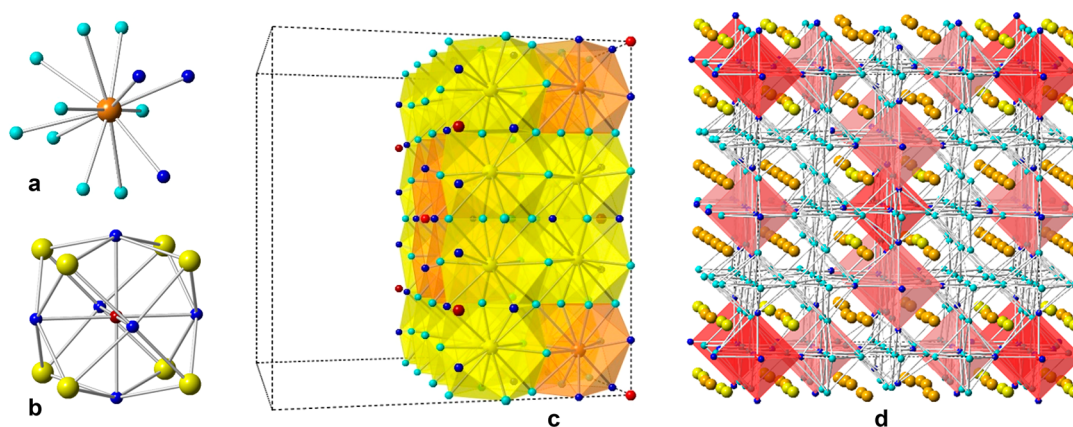
Figure 3. Coordination environments of sites in $U_8Al_{19}Si_6$. (a) Distorted cuboctohedral coordination of uranium sites. (b) Octahedral coordination of stuffed sites. (c) Segment of the unit cell with $U@X_{12}$ coordination shown as polyhedra. (d) Unit cell with octahedral coordination of stuffed sites shown in red.

In the presence of alumina powder or cement UO_2 readily reacts to form the title compound, which grows as silver cubes or faceted spheroids that range from 0.2 to 2.5 mm in diameter. $U_8Al_{19}Si_6$ is produced from reactions of 0.5 mmol UO_2 with 1−4 mmol Si in 30 mmol Al. The largest crystals were grown using 2 mmol Si; however, the greatest yield came from using 4 mmol Si (50% yield, based on UO_2 reactant; UAl_x compounds were likely byproducts and dissolved in the 5 M NaOH). $U_8Al_{19}Si_6$ is stable to air; no oxidation or degradation is apparent under a light microscope after months of air exposure. It is also stable to water, 5 M aqueous sodium hydroxide, and 1 M aqueous hydrochloric acid.

Structure. $U_8Al_{19}Si_6$, a new stuffed supercell variant of UAl_3, crystallizes in the $Pm\bar{3}n$ space group. Its relationship to the parent compound is depicted in Figure 2. It exhibits a 4-fold expansion along each axis ($a' = 4a_c$, where a_c is the UAl_3 unit cell) and occupancy of two additional crystallographic sites. In order to accommodate these "stuffed" sites, the surrounding atoms shift away from them; this leads to wave-like patterns of atoms when viewed down the cell axes. Another supercell of UAl_3 that has been previously reported to form upon partial substitution of silicon is the tetragonal symmetry $U(Al_{3-x}Si_x)$ structure with $a_t = 2a_c$ and $c_t = 4a_c$; this is also shown in Figure

2.[14,15] This structure is only observed for stoichiometries from $UAl_{1.2}Si_{1.8}$ to $UAl_{1.74}Si_{1.26}$ and it contains no extra stuffed sites; the tetragonal supercell is postulated to form due to some preferential siting of aluminum and silicon, although the siting could not be refined.

All of these structural variants—UAl_3, the tetragonal $U(Al_{3-x}Si_x)$ supercell, and the new cubic structure $U_8Al_{19}Si_6$—feature uranium atoms coordinated by 12 light atoms (X = Al or Si). This coordination is a perfect cuboctahedron in the parent compound, and increasingly distorted going from the tetragonal supercell to the cubic stuffed supercell. $U_8Al_{19}Si_6$ has two crystallographically unique uranium sites, with U−X bond distances ranging from 2.854(2)Å to 3.076(3)Å. There is an evident gap in bond lengths in the middle of this range for each uranium site; therefore, all X atoms with U−X distances equal to or shorter than 2.888(1)Å were assigned as silicon, and all X atoms with U−X distances equal to or longer than 2.964(4)Å were assigned as aluminum. This is in agreement with the observed U−X bond lengths in the parent compounds (2.853 Å in USi_3, and 3.016 Å in UAl_3).[13] Each uranium site in $U_8Al_{19}Si_6$ is surrounded by 9 aluminum atoms and 3 silicon atoms, with the
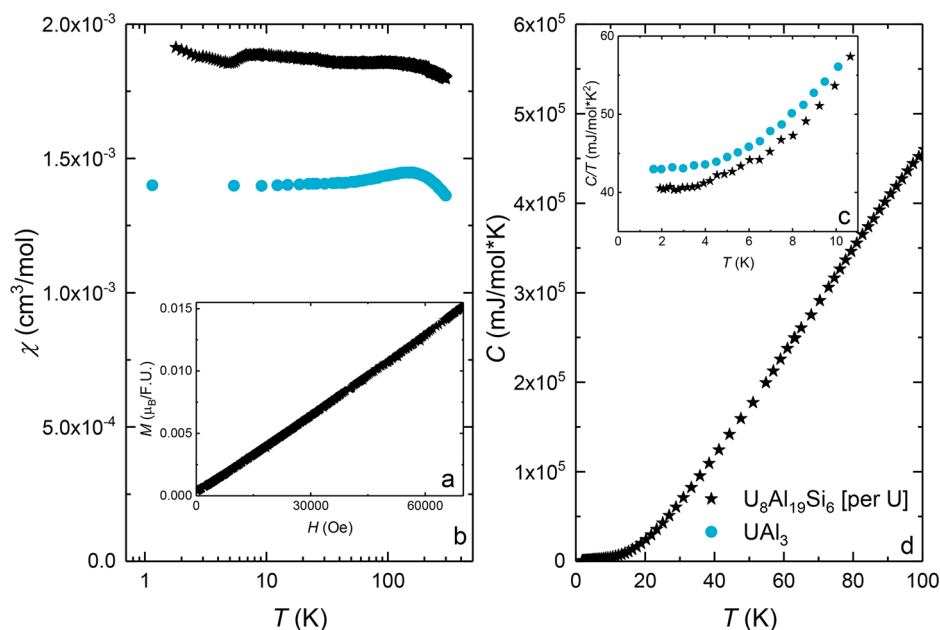
Figure 4. Magnetization and heat capacity data for $U_8Al_{19}Si_6$, calculated for formula unit $U(Al/Si)_{3.125}$. (a) M vs H data collected at 1.8 K. (b) Magnetic susceptibility of $U(Al/Si)_{3.125}$ (black) compared to data reported for UAl_3 (blue).[34] (c) Low temperature heat capacity C/T vs T of $U(Al/Si)_{3.125}$ (black) compared to that of UAl_3 (blue).[17] (d) Heat capacity data for $U(Al/Si)_{3.125}$.

3 silicon atoms all positioned on one triangular face of the distorted cuboctahedral coordination environment.

It is unfortunately not possible to decisively determine Al vs Si siting, or rule out Al/Si site mixing, based on X-ray diffraction data alone; the X-ray scattering factor of these two elements is too similar. However, their neutron scattering lengths vary by over 15%.[29] Single crystal neutron diffraction data were collected at 150 K to further explore the occupancies of the light element sites. The data indicate that the majority of the sites are preferentially occupied by only one type of atom, and the assignments based on bond lengths are correct. There does appear to be one mixed site; Al3 is occupied by 86% Al and 14% Si. Partial occupancy was also indicated for one of the stuffed sites: Al8 (on the 2a Wyckoff site) refines as 91% occupied. Taking into account these results, the precise stoichiometry is $U_8Al_{18.56}Si_{6.42}$, but the formula $U_8Al_{19}Si_6$ will be used as a shorthand.

The neutron diffraction data was also used to explore the possibility of interstitial hydride incorporation from reaction with hydroxyl groups on the high surface area alumina required to form the compound. The map of nuclear density was investigated for negative scattering peaks corresponding to ^1H nuclei at interstitial positions. Only two likely candidate sites were found (see Table S2 and Figure S2, Supporting Information), but the refined occupancies are below 10% and the overall refinement is not significantly improved by their incorporation into the model. It is therefore possible that hydride is present in the compound in trace amounts. However, given the difficulty in detecting hydrogen using diffraction methods, additional studies are required to verify this.

The occupancy of the two stuffed sites (Al7 and Al8, on high symmetry Wyckoff sites 2a and 6c) distinguishes the title compound from other UAl_3 superstructures. These positions are each octahedrally coordinated by six silicon sites at distances of 2.613(3) − 2.621(2)Å, as shown in Figure 3. This bond length is slightly long for a Si−Si bond (which generally fall in the 2.3−2.5 Å range) but is well within the

range expected for Al−Si bonds in intermetallic compounds (2.5−2.7 Å).[9−13] Both stuffed sites were therefore assigned as aluminum; this was supported by the neutron diffraction refinement. The resulting stoichiometry of $U_8Al_{19}Si_6$ has a $UX_{3.125}$ ratio, in accordance with it being a "stuffed" variant of UAl_3. The distortion of the UAl_3 parent structure to accommodate these additional sites is particularly clear when the $U@X_{12}$ coordination environments are shown in polyhedral mode; see Figure 3.

The relationship of the UAl_3 parent structure to that of perovskite sheds further light on the stuffed sites observed in $U_8Al_{19}Si_6$. UAl_3 (with the Cu_3Au structure type) can be viewed as a defect perovskite (ABO_3), with uranium on the A cation site, aluminum on the oxygen site, and the octahedrally coordinated B cation site being vacant. In the structure of $U_8Al_{19}Si_6$, 1/8 of these octahedral sites are filled (shown in Figure 3d). Several other intermetallic structures can be viewed as "stuffed" Cu_3Au structure types; these include $TmMn_xGa_3$, Y_4CrGa_{12}, and $Y_4Mn_{1−x}(Ga/Ge)_{12}$.[30−32] The different stuffing patterns of the extra atoms in these structures leads to different unit cell sizes, symmetries, and overall stoichiometries. $U_8Al_{19}Si_6$ exhibits a new stuffing pattern and accordingly a new supercell. Chemical pressure likely plays a significant role in the ordered positioning of the silicon sites around the stuffed positions; the shorter U−Si bonds allow for larger octahedral sites which can incorporate the additional aluminum atoms.[33]

Electronic Properties. Magnetic susceptibility data were collected for several different single crystal specimens of $U_8Al_{19}Si_6$. Temperature independent Pauli paramagnetism is consistently seen at high temperature, indicating the absence of a localized magnetic moment on uranium. The magnitude of the molar susceptibility χ (0.0018 emu/mol when calculated per mole of $U(Al/Si)_{3.125}$) is similar in magnitude to that reported for UAl_3 (0.0014 emu/mol),[34] which is consistent with the idea that $U_8Al_{19}Si_6$ behaves as a stuffed substituted variant of UAl_3. All $U_8Al_{19}Si_6$ samples show a small and sample dependent splitting of the field-cooled and zero-field cooled

susceptibilities below 100 K and a sharper feature below 7 K (Figure S3). Low temperature field dependence data (M vs H curves) are linear up to 7 T, but show a small amount of hysteresis at low fields (Figure 4a). The origin of these hysteretic features is not clear, but given that it is sample dependent, we suggest that it might come from a small impurity of the sample. This is supported by single crystal neutron diffraction data collected above and below these temperatures, which shows no additional peaks or peak intensity changes, shifts, or splitting. This indicates that there is no long-range magnetic ordering or structure change.

The temperature dependence of the heat capacity of $U_8Al_{19}Si_6$ (calculated for formula unit $U(Al/Si)_{3.125}$) is shown in Figure 4c,d. We first note that there are no distinct features that would be associated with possible phase transitions. This reinforces the idea that the sample dependent and hysteretic features that are seen in the magnetic susceptibility data are not indicative of bulk behavior. At low temperatures, the C/T of $U(Al/Si)_{3.125}$ is similar to that of UAl_3 and follows a temperature dependence consistent with Fermi liquid behavior, although further measurements (e.g., electrical transport) are needed to verify this. Fitting of the data to the expression $C/T = \gamma + \beta T^2$ yield $\gamma = 40.32$ mJ/(mol·K^2)^2 and $\beta = 0.13$ mJ/(mol·K^4)^4, which are comparable to values observed for UAl_3.[17] This further reinforces the conclusion that $U_8Al_{19}Si_6$ should be considered as a stuffed variant of UAl_3, where the electronic state is characterized as a mass enhanced Pauli paramagnet.

CONCLUSION

A new U/Al/Si ternary intermetallic has been isolated from the reaction of UO_2 and silicon in aluminum flux. This reaction is dependent on the nature of the alumina present in the reaction mixture (the crucible walls, alumina cement, or added alumina powder), indicating surface hydroxides may promote the formation of $U_8Al_{19}Si_6$ over $U(Al_{3-x}Si_x)$ compounds. The structure of $U_8Al_{19}Si_6$ is a stuffed supercell of Cu_3Au-type UAl_3; neutron diffraction data confirms that it exhibits aluminum and silicon ordering. The specific ratio and ordering of longer U−Al and shorter U−Si bonds may create chemical pressure that induces the incorporation of stuffed sites; attempts to make a germanium analogue by reacting UO_2 and germanium in aluminum flux have not been successful. The uranium in $U_8Al_{19}Si_6$ does not have a magnetic moment. Syntheses of thorium and plutonium analogues are being investigated.

ASSOCIATED CONTENT

ⓈSupporting Information

The Supporting Information is available free of charge on the ACS Publications website at DOI: 10.1021/acs.chemmater.8b00948.

> Table of atomic coordinates and thermal parameters for $U_8Al_{19}Si_6$ crystal from SCXRD collected at 158 K; powder diffraction data for $U_8Al_{19}Si_6$ collected at 293 K; table of atomic coordinates including possible hydride sites and figure depicting hydride coordination environments; and magnetic susceptibility data for several samples (PDF)
> Crystallographic data (CIF)

AUTHOR INFORMATION

ORCID ⓘ
Susan E. Latturner: 0000-0002-6146-5333

Notes
The authors declare no competing financial interest.

REFERENCES

(1) Leenaers, A.; Detavernier, C.; Van den Berghe, S. The effect of silicon on the interaction between metallic uranium and aluminum: A 50 year long diffusion experiment. *J. Nucl. Mater.* 2008, 381 (3), 242−248.

(2) Haertling, C.; Hanrahan, R. J. Literature review of thermal and radiation performance parameters for high-temperature, uranium dioxide fueled cermet materials. *J. Nucl. Mater.* 2007, 366 (3), 317−335.

(3) Gubbels, G. H. M.; Wolff, L. R. A Thermionic Energy Converter with a Molybdenum Alumina CERMET Emitter. *Proceedings of the 23rd Intersociety Energy Conversion Engineering Conference*; The American Society of Mechanical Engineers: 1988; pp 617−619.

(4) Kanatzidis, M. G.; Pöttgen, R.; Jeitschko, W. The metal flux: A preparative tool for the exploration of intermetallic compounds. *Angew. Chem., Int. Ed.* 2005, 44, 6996−7023.

(5) Phelan, W. A.; Menard, M. C.; Kangas, M. J.; McCandless, G. T.; Drake, B. L.; Chan, J. Y. Adventures in crystal growth: Synthesis and characterization of single crystals of complex intermetallic compounds. *Chem. Mater.* 2012, 24, 409−420.

(6) Latturner, S. E. Clusters, Assemble: Growth of Intermetallic Compounds from Metal Flux Reactions. *Acc. Chem. Res.* 2018, 51, 40−48.

(7) Canfield, P. C.; Kong, T.; Kaluarachchi, U. S.; Jo, N. H. Use of frit-disk crucibles for routine and exploratory solution growth of single crystalline samples. *Philos. Mag.* 2016, 96, 84−92.

(8) Latturner, S. E.; Kanatzidis, M. G. Formation of Multinary Intermetallics from Reduction of Perovskites by Aluminum Flux: $M_3Au_{6+x}Al_{26}Ti$ (M = Ca, Sr, Yb), a Stuffed Variant of the $BaHg_{11}$ Type. *Inorg. Chem.* 2004, 43 (1), 2−4.

(9) Ma, X.; Whalen, J. B.; Cao, H.; Latturner, S. E. "Competing phases, complex structure, and complementary diffraction studies of $R_3FeAl_{4-x}Mg_xTt_2$ intermetallics.". *Chem. Mater.* 2013, 25, 3363−3372.

(10) Latturner, S. E.; Kanatzidis, M. G. $REAu_4Al_8Si$: the end member of a new homologous series of intermetallics featuring thick $AuAl_2$ layers. *Chem. Commun.* 2003, 18, 2340−2341.

(11) Ma, X.; Chen, B.; Latturner, S. E. Synthesis and properties of new multinary silicides $R_5Mg_5Fe_4Al_{(x)}Si_{(18-x)}$ (R = Gd, Dy, Y; x = 12) grown in Mg/Al flux. *Inorg. Chem.* 2012, 51, 6089−6095.

(12) Latturner, S. E.; Bilc, D.; Mahanti, S. D.; Kanatzidis, M. G. Quaternary Intermetallics Grown from Molten Aluminum: The Homologous Series $Th_2(Au_xSi_{1-x})[AuAl_2]_nSi_2$ (n = 1, 2, 4). *Chem. Mater.* 2002, 14, 1695−1705.

(13) Villars, P.; Calvert, L. D. *Pearson's handbook of crystallographic data for intermetallic phases*; American Society for Metals: Metals Park, OH, 1986.

(14) Zenou, V. Y.; Rafailov, G.; Dahan, I.; Kiv, A.; Meshi, L.; Fuks, D. Ordered U(Al, Si)$_3$ phase: Structure and bonding. *J. Alloys Compd.* 2017, 690, 884−889.

(15) Rafailov, G.; Dahan, I.; Meshi, L. New ordered phase in the quasi-binary UAl_3–USi_3 system. *Acta Crystallogr., Sect. B: Struct. Sci., Cryst. Eng. Mater.* **2014**, *70* (3), 580–585.

(16) Dwight, A. E. *A Study of the Uranium-Aluminum-Silicon system*; Report ANL-82-14; Argonne National Laboratory: 1982.

(17) Cornelius, A.; Arko, A.; Sarrao, J.; Thompson, J.; Hundley, M.; Booth, C.; Harrison, N.; Oppeneer, P. Electronic properties of UX_3 (X = Ga, Al, and Sn) compounds in high magnetic fields: Transport, specific heat, magnetization, and quantum oscillations. *Phys. Rev. B: Condens. Matter Mater. Phys.* **1999**, *59* (22), 14473–14483.

(18) Ott, H. R.; Hulliger, F.; Rudigier, H.; Fisk, Z. Superconductivity in uranium compounds with Cu_3Au structure. *Phys. Rev. B: Condens. Matter Mater. Phys.* **1985**, *31* (3), 1329–1333.

(19) Onuki, Y.; Settai, R.; Shishido, H.; Ikeda, S.; Matsuda, T. D.; Yamamoto, E.; Haga, Y.; Aoki, D.; Harima, H.; Yamagami, H. Fermi surface properties and unconventional superconductivity in rare earth, uranium and transuranium compounds. *J. Optoelectron. Adv. Mater.* **2008**, *10*, 1535–1563.

(20) Sheldrick, G. M. *SHELXTL NT/2000*, Version 6.1; Bruker AXS: Madison, WI, U.S.A., 2000.

(21) Chakoumakos, B. C.; Cao, H.; Ye, F.; Stoica, A. D.; Popovici, M.; Sundaram, M.; Zhou, W.; Hicks, J. S.; Lynn, G. W.; Riedel, R. A. Four-circle single-crystal neutron diffractometer at the High Flux Isotope Reactor. *J. Appl. Crystallogr.* **2011**, *44* (3), 655–658.

(22) Rodriguez-Carvajal, J. FULLPROF. *Phys. B* **1993**, *192*, 55.

(23) Yan, J. Q. Flux growth utilizing the reaction between flux and crucible. *J. Cryst. Growth* **2015**, *416*, 62–65.

(24) Dickman, M. J.; Latturner, S. E. Metal nitrides grown from Ca/Li flux: $Ca_6Te_3N_2$ and new nitridoferrate(I) $Ca_6(Li_xFe_{1-x})Te_2N_3$. *J. Am. Chem. Soc.* **2016**, *138*, 10636–10644.

(25) Zhou, S.; Latturner, S. E. $Nd_8Co_{4-x}Al_xGe_2C_3$: A case study in flux growth of lanthanide-rich intermetallics. *J. Solid State Chem.* **2016**, *236*, 159–165.

(26) Heemeier, M.; Frank, M.; Libuda, J.; Wolter, K.; Kuhlenbeck, H.; Baumer, M.; Freund, H. The Influence of OH Groups on the Growth of Rhodium on Alumina: A Model Study. *Catal. Lett.* **2000**, *68* (1–2), 19–24.

(27) Jensen, M. C. R.; Venkataramani, K.; Helveg, S.; Clausen, B. S.; Reichling, M.; Besenbacher, F.; Lauritsen, J. V. Morphology, Dispersion, and Stability of Cu Nanoclusters on Clean and Hydroxylated α-Al_2O_3(0001) Substrates. *J. Phys. Chem. C* **2008**, *112*, 16953–16960.

(28) Sterrer, M.; Freund, H. J. Towards Realistic Surface Science Models of Heterogeneous Catalysts: Influence of Support Hydroxylation and Catalyst Preparation Method. *Catal. Lett.* **2013**, *143*, 375–385.

(29) Sears, V. F. Neutron scattering lengths and cross sections. *Neutron News.* **1992**, *3* (3), 26–37.

(30) Fulfer, B. W.; McAlpin, J. D.; Engelkemier, J.; McCandless, G. T.; Prestigiacomo, J.; Stadler, S.; Fredrickson, D. C.; Chan, J. Y. Filling in the Holes: Structural and Magnetic Properties of the Chemical Pressure Stabilized $LnMn_xGa_3$ (Ln = Ho–Tm; x < 0.15). *Chem. Mater.* **2014**, *26* (2), 1170–1179.

(31) Slater, B. R.; Bie, H.; Stoyko, S. S.; Bauer, E. D.; Thompson, J. D.; Mar, A. Rare-earth chromium gallides RE_4CrGa_{12} (RE = Tb–Tm). *J. Solid State Chem.* **2012**, *196*, 409–415.

(32) Francisco, M. C.; Malliakas, C. D.; Piccoli, M. B.; Gutmann, M. J.; Schultz, A. J.; Kanatzidis, M. G. Development and Loss of Ferromagnetism Controlled by the Interplay of Ge Concentration and Mn Vacancies in Structurally Modulated $Y_4Mn_{1-x}Ga_{12-y}Ge_y$. *J. Am. Chem. Soc.* **2010**, *132* (26), 8998–9006.

(33) Fredrickson, D. C. DFT-Chemical Pressure Analysis: Visualizing the Role of Atomic Size in Shaping the Structures of Inorganic Materials. *J. Am. Chem. Soc.* **2012**, *134*, 5991–5999.

(34) Aoki, D.; Watanabe, N.; Inada, Y.; Settai, R.; Sugiyama, K.; Harima, H.; Inoue, T.; Kindo, K.; Yamamoto, E.; Haga, Y.; Onuki, Y. Fermi surface properties of the enhanced Pauli paramagnet UAl_3. *J. Phys. Soc. Jpn.* **2000**, *69* (8), 2609–2614.